

Evidence for subdominant multipole moments and precession in merging black-hole-binaries from GWTC-2.1

Charlie Hoy,¹ Cameron Mills,^{1,2,3} and Stephen Fairhurst¹

¹*School of Physics and Astronomy, Cardiff University, Cardiff, CF24 3AA, United Kingdom*

²*Albert-Einstein-Institut, Max-Planck-Institut für Gravitationsphysik, D-30167 Hannover, Germany*

³*Leibniz Universität Hannover, D-30167 Hannover, Germany*

(Dated: April 22, 2022)

The LIGO–Virgo–KAGRA collaborations (LVK) produced a catalogue containing gravitational-wave (GW) observations from the first half of the third GW observing run (O3a). This catalogue, GWTC-2.1, includes for the first time a number of *exceptional* GW candidates produced from merging black-hole-binaries with unequivocally unequal component masses. Since subdominant multipole moments and spin-induced orbital precession are more likely to leave measurable imprints on the emitted GW from unequal component mass binaries, these general relativistic phenomena may now be measurable. Indeed, both GW190412 and GW190814 have already shown conclusive evidence for subdominant multipole moments. This provides valuable insights into the dynamics of the binary. We calculate the evidence for subdominant multipole moments and spin-induced orbital precession for all merging black-hole-binaries in GWTC-2.1 that were observed during O3a and show that (a) no gravitational-wave candidate has measurable higher order multipole content beyond $\ell = 3$, (b) in addition to the confident subdominant multipole measurements in GW190412 and GW190814, GW190519_153544 and GW190929_012149 show marginal evidence for the $(\ell, |m|) = (3, 3)$ subdominant multipole, (c) GW190521 may have measurable subdominant multipole content and (d) GW190412 may show evidence for spin-induced orbital precession.

I. Introduction

Between 2015 and 2017, the Advanced LIGO [1] (aLIGO) and Advanced Virgo [2] (AdV) gravitational-wave (GW) detectors performed their first and second GW observing runs (O1 and O2). During this time, the LIGO Scientific and Virgo collaborations (LVC) announced GWs originating from ten binary-black-hole (BBH) mergers [3–9] and a single binary neutron star [10]. Additional compact binary candidates have also been reported by other groups [11–14].

The observed signals match well with the predictions of general relativity, calculated using accurate waveforms modelled to fit predictions from post-Newtonian methods and numerical relativity simulations. However, two important general relativistic effects, higher order multipoles [15] and spin-induced orbital precession [16] were not clearly identified in the signals observed during O1 and O2 [9, 17, 18].¹ The gravitational wave emitted during a binary merger can be decomposed into a set of spin-weighted spherical harmonics [15]. The majority of the gravitational wave signal is contained in the quadrupole mode, $(\ell, m) =$

$(2, 2)$. Higher order multipoles are present for all binary systems, but they are typically at a much lower amplitude than the quadrupole [see e.g. 22]. Spin-induced orbital precession arises when there is a misalignment between the orbital angular momentum and the spins of each compact object leading to characteristic modulations in the amplitude and phase of the observed GW signal [16]. Including both higher order multipoles and precession in waveform models that are used to infer source properties through Bayesian inference [see e.g. 23–25] can improve parameter measurement accuracy and provide additional constraints on the in-plane spin components of the binary [see e.g. 26–30]. The importance of both of these effects increase as the binary’s mass ratio ($q = m_1/m_2 \geq 1$) increases [22, 30–37]. Clear evidence for asymmetric masses was absent in the binaries detected during O1 and O2 [9], making the observation of either precession and higher order multipoles challenging.

An initial analysis of the first 6 months of data from the first half of the third GW observing run (O3a) by the LIGO-Scientific, Virgo and KAGRA collaborations (LVK) revealed a further 39 GW candidates described in the second GW catalogue (GWTC-2) [38]. Subsequent searches over the same period revealed a number of subthreshold candidates [39, 40], with the extended second GW catalogue, (GWTC-2.1), increasing the number of high-significance GW candidates observed during O3a to a total of 44 [40]. Recently, the LVK

¹ See Refs. [19, 20] for a discussion regarding marginal evidence for higher order multipoles in GW170729 [9], and Ref. [21] for discussion of evidence for higher modes and precession in GW151226.

released the third GW catalogue (GWTC-3), which analysed the second half of the third GW observing run (O3b) and found a further 35 GW candidates [41].

In contrast to O1 and O2, several events in O3 had unequivocally unequal masses. First among these is GW190412 [28], with a mass ratio of $\sim 4:1$. The unequal mass ratio resulted in more significant higher order multipoles, and for the first time, imprints of subdominant multipole radiation oscillating at three times the orbital frequency – the $(\ell, m) = (3, 3)$ multipole² – were visible. Similarly, it was the first time that the in-plane spins, which lead to precession in the system, were constrained away from the prior [28, 39, 42–44]. Several months later GW190814 was detected with highly asymmetric component masses ($\sim 9:1$) and a secondary component with a mass larger than any previously discovered neutron star and lighter than any black hole [29]. GW190814 had significant evidence of the $(3,3)$ multipole [29, 44] and the most restrictive measurement of the in-plane spin components of any event observed to date. A combination of the higher order multipoles and the lack of evidence for precession reduced the uncertainty on the mass of the smaller object.

By comparing parameter estimates that were obtained with waveform models that a) included higher order multipoles and b) excluded higher order multipoles beyond $\ell = 2$, it has been suggested that several GW signals in O3a show possible evidence for higher order multipoles [38]. Similarly, by comparing the posterior and prior distributions for parameters characterizing spin-induced orbital precession, it has previously been shown that no event in O3a or O3b unambiguously exhibits spin-induced orbital precession [38, 41] (although see Ref. [45] which discusses strong evidence for precession in a GW candidate observed in O3b), but there is evidence that the observed population of BBHs have spins which are misaligned with the orbital angular momentum [46, 47]. Other studies have investigated the evidence for higher order multipoles and precession for GW190412 and GW190814 [28, 29, 42–44]. To date, there has not been a study which quantifies the evidence for precession and higher order multipoles across all events on an event by event basis.

In this paper, we take advantage of the multipole decomposition for identifying the presence of higher order multipoles [22] and the two-harmonic formalism for identifying the presence of precession [18, 30, 48] to establish if any BBH candidates in GWTC-2.1, that were

observed during O3a, exhibit evidence for higher order multipoles and precession. We calculate the signal-to-noise ratio (SNR) in the $(\ell, m) \in \{(2, 1), (3, 3), (4, 4)\}$ multipoles and from precession for the latest BBH observations and compare then to the expected distribution from noise. We include GW190814 since it is most likely (71%) the result of a BBH merger [29]. We show that,

1. There is minimal evidence for GW emission in the subdominant multipole moments beyond $\ell = 3$,
2. GW190814 has the largest evidence for the $(\ell, m) = (3, 3)$ multipole for all events in O3a with SNR in the $(3, 3)$ multipole $\rho_{33} = 6.2_{-1.5}^{+1.3}$,
3. GW190814 and GW190412 show significant evidence for the $(3, 3)$ subdominant multipole moment while the evidence for GW190519_153544 and GW190929_012149 is marginal,
4. GW190521 may show evidence for subdominant multipole moments. The reanalysis of GW190521 by Nitz *et al.* [39] suggests evidence for the $(3, 3)$ multipole while the initial analysis by the LVK shows minimal evidence,
5. GW190412 and GW190915_235702 show marginal evidence for spin-induced orbital precession while the population shows no significant evidence of precession.

This paper is structured as follows: Section II details the method used to infer the presence of higher order multipoles and precession in the observed GW data. We provide a brief overview of the two-harmonic approximation and a summary of how the SNR from precession and each subdominant multipole is calculated. We then explain how we construct the expected noise distribution for both measurements. In Section III we present our results and indicate which GW events show evidence for subdominant multipoles and precession. We then conclude, in Section IV, with a summary and discussion of future directions.

II. Method

a. Calculating the SNR in precession and higher multipoles

In general relativity, GWs are fully described by two polarizations. These polarizations can be decomposed into multipole moments using the -2 spin-weighted spherical harmonic orthonormal basis [49]. Coalescing

² (ℓ, m) should everywhere be read as $(\ell, |m|)$ unless otherwise indicated.

compact binaries (CBCs) predominantly emit radiation at twice the orbital frequency in the leading order (2,2) multipole. The most important subdominant multipole for most CBCs is the (3,3) multipole, though the (4,4) multipole can be more significant for binaries whose components have comparable masses [22].

Previous studies have identified evidence for subdominant multipole moments by either a) calculating Bayes factors, the difference in Bayesian evidences, through multiple parameter estimation studies [e.g. 19, 42, 43] or via likelihood re-weighting [17], b) statistically comparing posteriors obtained with waveform models which included higher order multipoles and those which excluded higher order multipoles beyond $\ell = 2$ [50], c) analysing time-frequency tracks in the GW strain data [28, 51], d) identifying if there is a loss in the observed coherent signal energy when comparing the output from the cWB detection pipeline [52] with predictions from a waveform model which excludes subdominant multipole moments [29], or e) directly calculating the SNR of each (ℓ, m) multipole $\rho_{\ell m}$ [22, 28, 29, 53]. Here, we identify whether multipoles other than the dominant (2,2) multipole have been observed by calculating the orthogonal SNR of each (ℓ, m) multipole. This is achieved by decomposing a GW signal into each subdominant multipole, extracting the component that is orthogonal to the (2, 2) quadrupole and calculating the SNR associated with the resulting waveform.

A binary with spin angular momenta \mathbf{S}_1 and \mathbf{S}_2 undergoes spin-induced orbital precession when the total spin $\mathbf{S} = \mathbf{S}_1 + \mathbf{S}_2$ of the binary is misaligned with the Newtonian orbital angular momentum \mathbf{L} . In most cases, precession of the orbital plane leads to \mathbf{L} precessing around the approximately constant $\mathbf{J} = \mathbf{L} + \mathbf{S}$, leading to characteristic modulations in the emitted GW signal [16, 54].

Previous studies have identified evidence for spin-induced orbital precession by either a) calculating Bayes factors [e.g. 28, 29, 42, 55], b) statistically comparing posterior distributions for parameters characterizing precession to their prior distributions [e.g. 9, 50] or c) directly calculating the precession SNR, described as the contribution to the total SNR of the system that can be attributed to precession [18, 28–30, 37, 48, 50]. In this paper, we identify if spin-induced orbital precession has been observed from a GW signal by calculating the precession SNR. The precession SNR ρ_p is calculated by decomposing the (2,2) multipole into non-precessing harmonics, whose frequencies differ by multiples of the precession frequency, and isolating the SNR contained in the second most significant harmonic (see [48] for details). If ρ_p is small, the am-

plitude of the second harmonic is insignificant the observed waveform carries little imprint of orbital precession. In this case, we would observe a GW signal which looks like the dominant non-precessing harmonic. The precession SNR has been shown previously to accurately identify whether spin-induced orbital precession has been observed in simulated GW signals [30, 37].

The formalisms for $\rho_{\ell m}$ and ρ_p were initially developed for waveform models containing higher order multipoles [22] or precession [18, 48] respectively, but not both. In this paper, we apply them to posterior samples obtained with a gravitational waveform model containing both higher multipoles and precession. We heuristically justify this by noting that, in most cases, both precession and higher multipoles are small corrections to the leading order gravitational waveform. It is therefore reasonable to expect that the precession correction to the higher multipoles will be an even smaller effect which can be safely ignored. We leave a detailed derivation of this for future work [48]. Briefly, a GW signal containing only the $(\ell, m) = (2, 2)$ multipole can be written as a sum of 5 non-precessing harmonics, $h_{22} = \mathcal{A}_{22,0}h^{22,0} + \mathcal{A}_{22,1}h^{22,1} + \dots$, where $\mathcal{A}_{22,n}$ is the (complex) amplitude of the n th harmonic $h^{22,n}$ which depends upon the orientation of the signal. The amplitude of each harmonic scales with b^n where $b = \tan \beta/2$ and β is the opening angle (the polar angle between \mathbf{L} and \mathbf{J}). The characteristic amplitude and phase modulations associated with precession are caused by the beating of these 5 non-precessing harmonics. Since for the majority of cases $b \ll 1$, a GW signal containing only the $\ell = 2$ multipoles can approximately be written as a sum of the two leading harmonics, $h_{22} \approx \mathcal{A}_{22,0}h^{22,0} + \mathcal{A}_{22,1}h^{22,1}$. When the GW signal includes other multipoles, they can be decomposed similarly. For example, we can express $h_{33} \approx \mathcal{A}_{33,0}h^{33,0} + \mathcal{A}_{33,1}h^{33,1}$ where $\mathcal{A}_{33,n}$ is the amplitude of the n th harmonic $h^{33,n}$. As before, the amplitude of the precession harmonics scale as b^n . Furthermore, the overall amplitude of the (3,3) multipole is typically much lower than the (2,2) multipole. Therefore, to a good approximation, we can write the waveform as $h \approx \mathcal{A}_{22,0}h^{22,0} + \mathcal{A}_{22,1}h^{22,1} + \mathcal{A}_{33,0}h^{33,0}$. The $(\ell, m) = (4, 4)$ precession multipoles can be added in a similar fashion, although their amplitude is generally smaller than the (3,3) and can often be neglected. When computing ρ_p throughout this paper, we only consider the precession power in the leading (2, 2) multipole. Similarly, when calculating the power in higher multipoles, we consider only the contribution from, e.g., $h^{33,0}$ and neglect the precession corrections.

b. Calculating the expected distribution of ρ_p and $\rho_{\ell m}$ in the absence of a signal

In order to assess the significance of precession and higher order multipoles, we compare the inferred ρ_p and $\rho_{\ell m}$ distributions to the expected distribution from noise. Since the statistical properties of ρ_p and $\rho_{\ell m}$ are similar, the expected noise distribution has the same functional form for both measurements. Below we summarize the derivation of the common noise distribution (parameterized by ρ which denotes either ρ_p or $\rho_{\ell m}$) and we refer the reader to Refs. [22, 30] for further details.

We consider a gravitational waveform comprising

a dominant contribution h_0 , the leading precession harmonic of the (2,2) multipole, and a single, additional, subdominant contribution h_1 arising either from a higher multipole or from precession. The gravitational waveform can be written as

$$h = \mathcal{A}_0(\boldsymbol{\lambda})h_0(\boldsymbol{\lambda}) + \mathcal{A}_1(\boldsymbol{\lambda})h_1(\boldsymbol{\lambda}) \quad (1)$$

where $\mathcal{A}_i(\boldsymbol{\lambda})$ are overall amplitudes which depend upon the orientation of the binary, and $\boldsymbol{\lambda}$ denotes the parameters of the system [22, 48]. The GW likelihood may then be factorized into two components: one describing the contribution from the dominant harmonic, $\Lambda_0(\boldsymbol{\lambda})$, and another describing the contribution from the subdominant harmonic, $\Lambda_1(\boldsymbol{\lambda})$.

$$\begin{aligned} p(d|\boldsymbol{\lambda}) &\propto \exp\left(-\frac{1}{2}\langle d - [\mathcal{A}_0(\boldsymbol{\lambda})h_0(\boldsymbol{\lambda}) + \mathcal{A}_1(\boldsymbol{\lambda})h_1(\boldsymbol{\lambda})] | d - [\mathcal{A}_0(\boldsymbol{\lambda})h_0(\boldsymbol{\lambda}) + \mathcal{A}_1(\boldsymbol{\lambda})h_1(\boldsymbol{\lambda})] \rangle\right) \\ &\propto \exp\left(\mathcal{A}_0(\boldsymbol{\lambda})\langle d|h_0(\boldsymbol{\lambda}) \rangle - \frac{|\mathcal{A}_0(\boldsymbol{\lambda})|^2}{2}\langle h_0(\boldsymbol{\lambda})|h_0(\boldsymbol{\lambda}) \rangle\right) \times \exp\left(\mathcal{A}_1(\boldsymbol{\lambda})\langle d|h_1(\boldsymbol{\lambda}) \rangle - \frac{|\mathcal{A}_1(\boldsymbol{\lambda})|^2}{2}\langle h_1(\boldsymbol{\lambda})|h_1(\boldsymbol{\lambda}) \rangle\right) \\ &=: \Lambda_0(\boldsymbol{\lambda}) \times \Lambda_1(\boldsymbol{\lambda}) \end{aligned} \quad (2)$$

where d is the GW strain data. In the second line, we have absorbed the (constant) $\langle d|d \rangle$ term into the proportionality, and we have assumed that the dominant and subdominant harmonics are orthogonal $\langle h_0|h_1 \rangle = 0$.³

The phase evolution of the gravitational waveform, encoded in $h_{0,1}(\boldsymbol{\lambda})$, is determined by the masses and aligned spin components of the binary. Since the dominant harmonic has the largest SNR, its measurement will primarily be used to determine the evolution of the waveform. An observation of the sub-dominant harmonic will provide a small improvement to the evolution of the waveform. However, for simplicity, we neglect it in the following discussion. In this case, the subdominant harmonic h_1 is known and only the overall amplitude and phase, encoded in \mathcal{A}_1 remain to be determined. Furthermore, the value of \mathcal{A}_1 will typically be unconstrained by the observation of \mathcal{A}_0 — in the case of precession, both the amplitude and phase of \mathcal{A}_1 are free as they depend upon the in-plane spins,

while for higher multipoles the amplitude and phase of \mathcal{A}_1 will depend upon the orientation and mass ratio of the binary which are generally not precisely measured. Therefore, in the simplest approximation, we can simply maximize the likelihood $\Lambda_1(\boldsymbol{\lambda})$ over \mathcal{A}_1 ,

$$\Lambda_1(\boldsymbol{\lambda})_{\max} = \exp\left(\frac{[\rho_1^{\text{MF}}]^2}{2}\right) \quad (3)$$

where the matched filter SNR, ρ_1^{MF} is defined as

$$[\rho_1^{\text{MF}}]^2 = \frac{[(s|h_1)^2 + (s|ih_1)^2]}{|h_1|^2}. \quad (4)$$

$[\rho_1^{\text{MF}}]^2$ will be chi-squared distributed with two degrees of freedom in the absence of signal, and non-centrally chi-squared distributed in the presence of a signal. Using the maximum likelihood, a threshold of $\rho_1 \geq 2.1$ is a requirement for observation, at 90% confidence, of precession or higher multipoles (see Refs. [22, 48] for details).

Alternatively, we can marginalize the likelihood, $\Lambda_1(\boldsymbol{\lambda})$, over the unknown phase to obtain a likelihood as a function of ρ_1 as

$$\Lambda_1(\rho_1) \propto I_0(\rho_1^{\text{MF}} \rho_1) \exp\left(-\frac{[\rho_1^{\text{MF}}]^2 + \rho_1^2}{2}\right). \quad (5)$$

³ The calculation can be fairly simply generalized to the case where the harmonics are not orthogonal by simply replacing h_1 by h_1^\perp , the component of h_1 orthogonal to h_0 [22]. For ease of presentation, all calculations are in terms of h_1 but when we calculate $\rho_{\ell,m}$ and ρ_p in this work, we use h_1^\perp .

Here, I_0 is the Bessel function of the first kind. The expected posterior distribution for ρ_1 is, therefore,

$$p(\rho_1|d) \propto p(\rho_1) \Lambda_1(\rho_1), \quad (6)$$

where $p(\rho_1)$ is the prior distribution for ρ_1 . For the case of uniform priors on the complex amplitude \mathcal{A}_1 , $p(\rho_1|d)$ takes the form of a non-central χ distribution with 2 degrees of freedom with non-centrality parameter equal to ρ_1^{MF} .

As shown in Refs. [22, 30], we can obtain a better prediction for the posterior distribution $p(\rho_1|d)$, by using the measurement of the dominant harmonic, h_0 , to place a more informative prior on the strength of the sub-dominant harmonic. For instance, an observation of a close to equal mass or face-on binary reduces the expectation of observing higher harmonics or precession. Here, we construct an *informed prior* for $p(\rho_1)$ using results, where available, from a parameter estimation analysis that includes only the dominant multipole. This *informed prior* is what results from calculating $p(\rho_1|d)$ in Eq. (6) while taking $\Lambda_1(\rho_1) = 1$.⁴

c. Assessing the significance of precession and higher multipoles

We follow the method introduced in Refs. [22, 30] and calculate $\rho_{\ell m}$ and ρ_p from the inferred properties of each compact binary merger in O3a. To do this we use posterior samples from the GWTC-2.1 data release [57]. For GW candidates not included in the GWTC-2.1 data release, samples from the GWTC-2 data release [58] are used. Further details about the specific posterior samples used are in Appendix A. We use the parameters of each sample to generate the leading order precession and higher multipole contributions to the waveform and calculate $\rho_{\ell m}$ and ρ_p for the network at the time of the event. This calculation uses the conversion module publicly available in PESUMMARY [59].⁵

⁴ For precession there are additional parameters that must be marginalized over which are not inferred with dominant multipole models: the precession spin χ_p [56] and the precession phase. However, the inference of aligned spin and mass ratio does provide additional constraints on these parameters, and so rather than assuming the default prior on these parameters, we condition on the measured aligned spin and mass ratio.

⁵ When computing $\rho_{\ell m}$ we generate a non-precessing waveform (i.e. set the in-plane spin components to zero) and calculate the higher multipole SNR for that waveform. This is not exactly identical to the prescription above but, provided that the

To assess the significance of precession and higher multipoles in gravitational-wave signals, we calculate the probability that the observed $\rho_{\ell m}$ and ρ_p are caused by noise. In other words, we calculate the probability that the inferred $\rho_{\ell m}$ or ρ_p can be reproduced under the assumption that the *true* gravitational-wave signal contains only the dominant contribution h_0 and noise is solely responsible for reproducing h_1 .

We do not calculate ρ_1^{MF} directly from the data, but rather infer it from the parameter estimation results. In particular, we determine the value of ρ_1^{MF} which gives an expected posterior distribution $p(\rho_1|d)$ from Eqs. (5) and (6) that matches the $\rho_{\ell m}$ or ρ_p distribution inferred from the parameter estimation samples. We then calculate the probability of drawing ρ_1^{MF} or larger from the expected noise distribution in the absence of higher multipoles and precession, i.e. from a chi distribution with 2 degrees of freedom. In practice, we obtain the value of ρ_1^{MF} by minimising the Jensen-Shannon divergence (JSD) [60] between $p(\rho_1|d)$ and the inferred posterior.

III. Results

From the publicly released posterior samples, we are able to quantify the evidence of subdominant multipole moments and precession in the observed GW signal. Our analysis finds that several candidates in GWTC-2.1 show strong evidence for the presence of subdominant multipole moments and others show marginal evidence for precession. A summary of the main results is given in Table I.

We report the observed SNR in the (3, 3) multipole and precession for all events in GWTC-2.1. Where possible, we also provide the probability that the inferred SNR in the (3,3) multipole and from precession is caused by noise, P_{33} and P_p respectively. Although we calculate the SNR in the (2,1), (3,3) and (4,4) subdominant multipoles, we only report the evidence for the (3,3). This is because our analysis finds that the (3,3) multipole is the most significant sub-dominant multipole for every event except one in O3a. This is expected since, across the majority of the parameter space, the expected SNR in the (3,3) multipole is

$b \ll 1$, any differences will be small. In particular, precession adds a secular drift in the phase evolution of the waveform. However, as we only use the waveform to calculate the expected SNR in the higher multipoles (i.e. we do *not* matched filter against the data), this small phase difference will not impact the value of ρ_{33} .

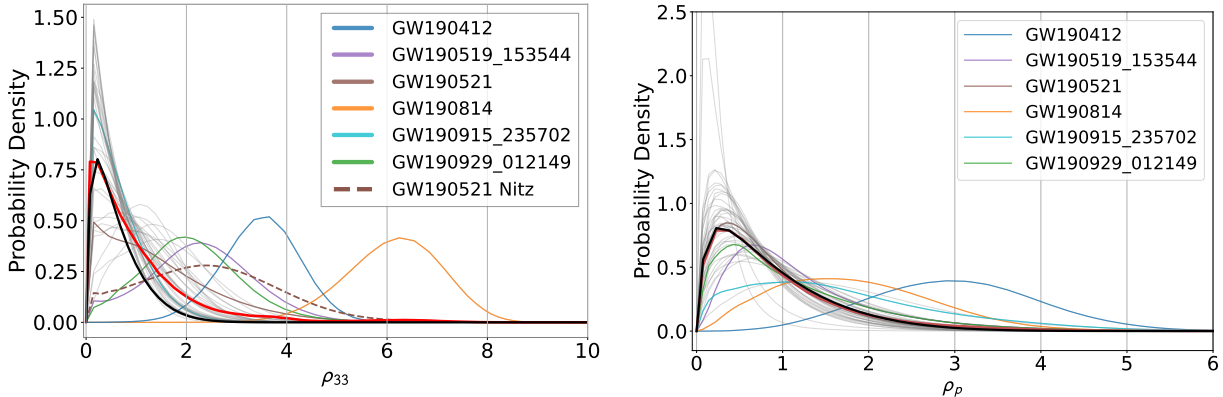


FIG. 1. Plot showing the *Left*: ρ_{33} and *Right*: ρ_p distributions for all observations in the second GW catalogue (grey). In red we show the ρ_{33} and ρ_p distribution averaged across events. In black we show the average of the median expected noise distribution for *Left*: higher multipoles and *Right*: precession. Events which are discussed in the text are colored.

largest. It is only binaries with a) large total mass – where the in-band power in the (4,4) is larger – and b) close to equal mass components – where the (3,3) multipole vanishes [22] – that the expected SNR in the (4,4) multipole is larger. GW190910.112807 is the sole exception, having inferred $\rho_{33} = 0.6^{+1.3}_{-0.6}$ and $\rho_{44} = 1.0^{+0.5}_{-1.0}$, both of which are consistent with noise with p-values $> 10\%$. As expected, GW190910.112807’s source has close to equal mass components, $q = m_1/m_2 = 1.22^{+0.48}_{-0.20}$, and has relatively large total mass $M = m_1 + m_2 = 79.6^{+9.3}_{-9.1} M_\odot$. It also has significant support for an edge-on orientation, where the relative amplitude of the (4,4) multipole is largest.

Several events in GWTC-2.1 have an SNR in the (3,3) multipole which is clearly above the expectation for noise alone. Indeed, the observed distribution for the population, shown in Figure 1, shows a clear high-SNR tail that indicates an observation of the (3,3) multipole. Higher multipoles have previously been identified in both GW190412 and GW190814, with their observability and their impact on parameter estimates discussed at length in previous works [28, 29, 42–44]. Unsurprisingly, we see that among all events in O3a, GW190412 and GW190814 have the largest SNRs in the (3, 3) multipole, with $\rho_{33} = 3.5^{+0.8}_{-1.2}$ and $\rho_{33} = 6.2^{+1.3}_{-1.5}$ respectively. For both events, the observed ρ_{33} is unlikely to be caused by noise since there is an approximately 1 in 400 and 1 in 6×10^7 chance that the observed distribution is caused by noise.

The events GW190519.153544 and GW190929.012149 show marginal evidence for an observable signal in the (3, 3) multipole. The observed SNRS are $\rho_{33} = 2.3^{+1.5}_{-1.8}$ and $\rho_{33} = 2.0^{+1.6}_{-1.5}$

respectively with associated p-values of $P_{33} = 1.6\%$ and $P_{33} = 4.2\%$ respectively. While a 1.6% p-value would be significant in a single trial, this is consistent with expectations when considering over thirty events from O3a.

The evidence for precession is weaker than for higher multipoles. As shown in Figure 1, there are only two events which show any significant deviation from the average expected noise distribution.

GW190412 shows the strongest evidence for precession with $\rho_p = 3.0^{+1.6}_{-1.5}$ and p-value 1.3%. Although significant in a single trial, this is consistent with expectations in a population of thirty events. While GW190814 has the second-largest precession SNR, $\rho_p = 1.8^{+1.6}_{-1.2}$, the observed distribution is consistent with zero precession: $P_p = 21\%$. We also find that GW190915.235702 shows marginal evidence for measurable precession with $\rho_p = 1.5^{+2.4}_{-1.2}$ and $P_p = 3.7\%$.

For the other events in GWTC-2.1, there is no evidence for precession since the inferred ρ_p is consistent with noise: $P_p > 10\%$.⁶ The lack of observable pre-

⁶ We note that two events, GW190602.175927 and GW190924.175927, have precession p-values $P_p = 100\%$. The reason that these events have such high p-values is because the inferred ρ_p is significantly lower than expected. This arises because ρ_p is calculated from an analysis incorporating both precession and higher harmonics, while the prior is generated from an analysis lacking both precession and higher harmonics. In both cases, the inclusion of higher harmonics significantly improves the estimate of the mass ratio and means that the prior distribution (of both mass ratio and ρ_p) is slightly different than the results of the precessing, higher-harmonic analysis.

Event	ρ_{33}	$P_{33}(\%)$	ρ_p	$P_p(\%)$
GW190403_051519	$1.4^{+1.3}_{-1.3}$	-	$0.3^{+0.9}_{-0.2}$	-
GW190408_181802	$0.5^{+1.1}_{-0.5}$	64.0	$1.0^{+1.8}_{-0.9}$	21.0
GW190412	$3.5^{+0.8}_{-1.2}$	0.24	$3.0^{+1.6}_{-1.5}$	1.3
GW190413_134308	$0.7^{+1.2}_{-0.6}$	62.0	$0.7^{+1.5}_{-0.6}$	15.0
GW190413_052954	$0.5^{+1.1}_{-0.5}$	11.0	$0.6^{+1.4}_{-0.5}$	40.0
GW190421_213856	$0.4^{+0.4}_{-0.9}$	95.0	$0.7^{+1.4}_{-0.6}$	24.0
GW190426_190642	$0.8^{+1.6}_{-0.7}$	-	$0.2^{+0.5}_{-0.2}$	-
GW190503_185404	$0.8^{+1.3}_{-0.7}$	21.0	$0.8^{+1.8}_{-0.7}$	28.0
GW190512_180714	$1.1^{+1.1}_{-0.9}$	19.0	$0.8^{+1.6}_{-0.7}$	59.0
GW190513_205428	$1.1^{+1.4}_{-1.0}$	24.0	$0.8^{+1.6}_{-0.6}$	71.0
GW190514_065416	$0.4^{+1.0}_{-0.4}$	39.0	$0.5^{+1.2}_{-0.4}$	28.0
GW190517_055101	$0.7^{+0.7}_{-0.7}$	39.0	$1.0^{+2.0}_{-0.8}$	31.0
GW190519_153544	$2.3^{+1.5}_{-1.8}$	1.6	$1.0^{+1.9}_{-0.7}$	13.0
GW190521	$1.2^{+2.4}_{-1.1}$	-	$0.7^{+1.4}_{-0.6}$	-
GW190521_074359	$1.0^{+1.5}_{-0.9}$	27.0	$1.6^{+2.5}_{-1.2}$	11.0
GW190527_092055	$0.6^{+1.1}_{-0.5}$	75.0	$0.7^{+1.7}_{-0.6}$	37.0
GW190602_175927	$0.8^{+1.4}_{-0.9}$	59.0	$0.5^{+1.0}_{-0.4}$	100.0
GW190620_030421	$1.1^{+1.5}_{-1.0}$	28.0	$0.8^{+1.7}_{-0.6}$	45.0
GW190630_185205	$1.0^{+1.2}_{-0.9}$	25.0	$1.0^{+1.8}_{-0.8}$	35.0
GW190701_203306	$0.5^{+1.0}_{-0.4}$	83.0	$0.5^{+1.0}_{-0.4}$	81.0
GW190706_222641	$1.5^{+1.5}_{-1.3}$	11.0	$0.5^{+1.1}_{-0.4}$	51.0
GW190707_093326	$0.4^{+0.8}_{-0.3}$	48.0	$0.7^{+1.5}_{-0.6}$	81.0
GW190708_232457	$0.4^{+0.9}_{-0.3}$	77.0	$0.7^{+1.5}_{-0.6}$	58.0
GW190719_215514	$0.7^{+1.2}_{-0.6}$	69.0	$0.6^{+1.5}_{-0.5}$	52.0
GW190720_000836	$0.5^{+0.9}_{-0.4}$	46.0	$0.6^{+1.2}_{-0.5}$	49.0
GW190725_174728	$0.5^{+1.0}_{-0.5}$	-	$1.0^{+1.9}_{-0.8}$	-
GW190727_060333	$0.5^{+1.2}_{-0.4}$	76.0	$0.7^{+1.6}_{-0.6}$	36.0
GW190728_064510	$0.5^{+1.2}_{-0.4}$	34.0	$0.7^{+1.3}_{-0.3}$	40.0
GW190731_140936	$0.5^{+1.1}_{-0.4}$	49.0	$0.5^{+0.9}_{-0.4}$	64.0
GW190803_022701	$0.4^{+0.9}_{-0.4}$	77.0	$0.6^{+1.4}_{-0.5}$	43.0
GW190805_211137	$0.6^{+1.1}_{-0.5}$	-	$0.5^{+1.2}_{-0.4}$	-
GW190814	$6.2^{+1.3}_{-1.5}$	1.7×10^{-6}	$1.8^{+1.6}_{-1.2}$	21.0
GW190828_063405	$0.5^{+1.0}_{-0.4}$	51.0	$0.9^{+1.6}_{-0.8}$	39.0
GW190828_065509	$1.2^{+1.0}_{-1.0}$	8.5	$1.0^{+1.9}_{-0.8}$	24.0
GW190910_112807	$0.6^{+1.3}_{-0.6}$	15.0	$0.8^{+1.6}_{-0.7}$	26.0
GW190915_235702	$0.5^{+1.0}_{-0.5}$	51.0	$1.5^{+2.4}_{-1.2}$	3.7
GW190916_200658	$0.8^{+1.3}_{-0.7}$	-	$0.5^{+1.2}_{-0.4}$	-
GW190924_021846	$0.5^{+1.0}_{-0.5}$	18.0	$0.5^{+1.1}_{-0.5}$	100.0
GW190925_232845	$0.3^{+0.8}_{-0.3}$	-	$0.7^{+1.3}_{-0.6}$	-
GW190926_050336	$0.8^{+1.4}_{-0.7}$	-	$0.7^{+1.7}_{-0.6}$	-
GW190929_012149	$2.0^{+1.6}_{-1.5}$	4.2	$0.9^{+2.0}_{-0.7}$	13.0
GW190930_133541	$0.4^{+1.0}_{-0.3}$	35.0	$0.6^{+1.2}_{-0.5}$	44.0

TABLE I. Table showing the SNR in the $(\ell, m) = (3, 3)$ multipole moment ρ_{33} and the SNR from precession ρ_p for all BBH candidates observed in GWTC-2.1 [40]. For each event we show two p-values; P_{33} and P_p show the probability that the inferred posterior is caused by noise. Events with a smaller p-value show greater evidence for higher order multipoles and/or precession. For events where the p-value and ρ_{33}/ρ_p could not be calculated we add a hyphen. Where applicable we report the median values along with the 90% symmetric credible intervals.

cession does not necessarily mean that most events in GWTC-2.1 have aligned-spins but rather that if the binaries were precessing, the imprint of precession on the observed signal is not strong enough to be observed with the current detector sensitivities.

Since GW190412, GW190814, GW190915_235702, GW190519_153544 and GW190929_01214 all show at least some evidence for the (3, 3) multipole or precession, we discuss these events in more detail in Section III b. We also discuss GW190521 since it has the largest inferred in-plane spin of all events in GWTC-2.1.

a. The population as a whole

First, we discuss the evidence for the (3, 3) multipole and precession in the population of observed GW candidates. In Figure 2 we plot the cumulative distribution of p-values for the (3, 3) multipole and for precession. If there was no-evidence for the (3, 3) multipole and/or precession in the population, we expect to observe a uniform distribution of p-values.

Our analysis finds strong evidence for the presence of the (3, 3) multipole in the population of GW candidates since the cumulative distribution of p-values lies outside of the 90% confidence interval of the no-signal hypothesis. We find that, as expected, both GW190412 and GW190814 are influential in this observation. When these two events are removed from the population, the cumulative distribution of p-values lies within the 90% confidence interval.

For the case of precession, we find no significant evidence for precession in the population of GW candidates and, overall, the population distribution for ρ_p is consistent with that expected from a non-precessing population. We note that the existence of misaligned spins has been inferred for this population, see e.g. Ref. [46]. However, these results are not necessarily incompatible as the requirement for misaligned spins can be driven by binaries with negative aligned spin, rather than in-plane spins.

For both the (3,3) multipole and precession analyses, we observe an excess of low significance events which have lower p-values than expected, see the upper-right of Figure 2. Indeed, at around a p-value of 0.5, the excess lies outside the 90% region for both ρ_{33} and ρ_p . Although apparent in both analyses, the excess is more significant for the precession analysis. We have not definitively identified the cause of this excess, but note several possible explanations. First, as discussed in Appendix A, for the majority of events the informed prior for the precession analysis is obtained using a

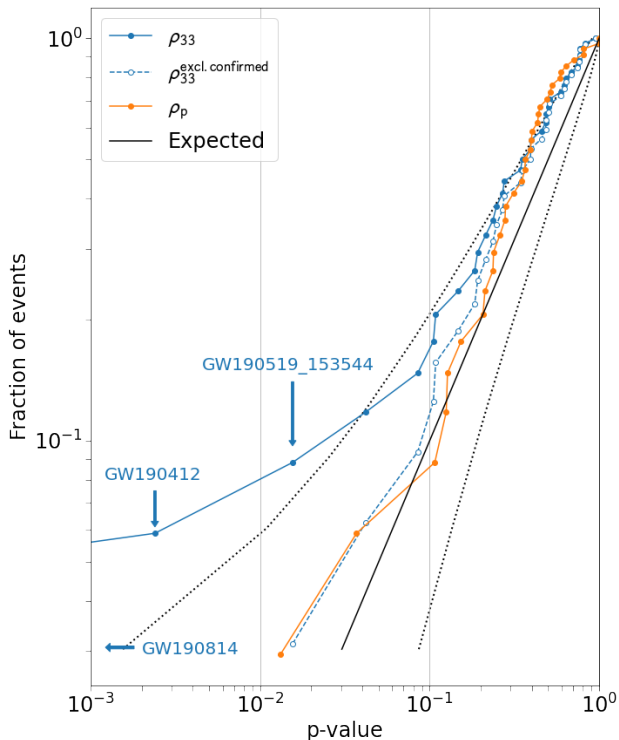


FIG. 2. The cumulative distribution of p-values for the evidence of subdominant multipole moments (solid blue) and precession (orange) for the gravitational-wave candidates observed in GWTC-2.1. The solid black line indicates the expected distribution of p-values under a no-evidence hypothesis with the corresponding 90% uncertainty band shown by the dotted black lines. The blue dashed line shows the cumulative distribution of p-values for the evidence of subdominant multipole moments when GW190412 and GW190814 are excluded from the population. The p-values for the evidence of subdominant multipole moments for GW190412, GW190519_153544 and GW190814 are labelled.

waveform model that lacks both precession and higher multipoles. Ideally, we would use results from an analysis which differed only in its treatment of precession, but none is available in the public data. This could lead to an incorrect estimate of the informed prior and consequently the p-value. Second, as discussed in Section II b, when deriving the form of the expected posterior in Eq. 6, we assume that the masses and aligned spins are measured exactly from the (2,2) waveform. In reality, this is not the case and could lead to small differences in the inferred p-values. Finally, the result could be genuine, in that this is a genuine statistical fluctuation – it is not unreasonable to observe an excess outside of the 90% confidence interval. In fact, the generic

expectation is that both the (3,3) and precessing harmonics will usually be present in the data but buried in the noise. The combination of a sub-threshold signal and noise is more likely to lead to excesses such as the one we observe here. It is worth noting, however, that this excess at high p-values does not impact our overall conclusions or the robustness of results at low p-values.

b. Individual GW candidates

Here, we discuss in more detail all GW candidates for which the p-value for higher multipoles or precession (or both) is less than 5%.

1. GW190814

GW190814 is the most unequal mass ratio binary observed in O3a. The component masses were inferred to be $23.2^{+1.1}_{-1.0} M_{\odot}$ and $2.59^{+0.08}_{-0.09} M_{\odot}$ which makes the secondary component mass either the heaviest neutron star or lightest black hole ever recorded. Previously, GW190814 was found to have significant evidence for subdominant multipole moments owing to the unequal component masses [29].

Unsurprisingly, we infer that GW190814 has the most significant measurement of ρ_{33} in O3a. We find that the inferred ρ_{33} measurement is inconsistent with noise since the associated p-value is significantly smaller than 1% and is the smallest for any event in O3a, $P_{33} = 1.7 \times 10^{-6}\%$.

Although GW190814 has the second largest ρ_p , there is minimal for precession in the observed GW signal. The inferred ρ_p measurement can be reproduced from noise in 21% of cases, as shown in Figure 3. GW190814 is an example where a large inferred ρ_p does not correlate with observable precession. Since this binary has highly unequal masses, a small in-plane spin would lead to observable precession. Therefore, our prior belief is that large values of ρ_p are quite possible — this differs from an equal mass binary for which it is very unlikely to obtain a large ρ_p . Consequently, GW190814’s inferred ρ_p distribution is well contained within the 1σ noise uncertainty, see Figure 3. GW190814 therefore demonstrates the efficacy of our algorithm for inferring the presence of precession.

The lack of observable precession in GW190814 implies that its source is either non-precessing or we are unable to observe the precession at current detector sensitivities. This is a similar conclusion to that stated in Ref. [37] which highlighted that a precessing

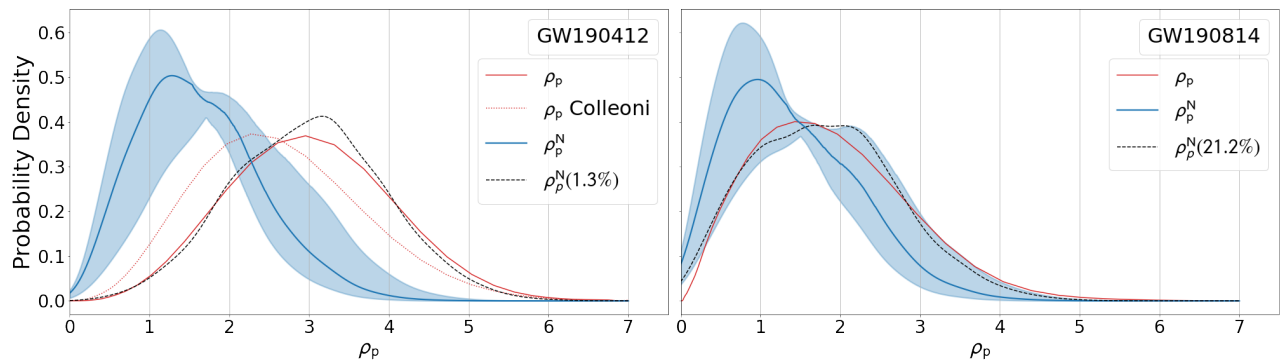


FIG. 3. ρ_p distributions for *Left*: GW190412 and *Right*: GW190814. The blue line shows the expected distribution of ρ_p in a stretch of noisy data under the assumption that the source is non-precessing, ρ_p^N . The blue shaded region shows the 1σ uncertainty of ρ_p^N and the black dashed line shows the expected ρ_p^N distribution in *Left*: 1.3% and *Right*: 21.2% of cases. The black dashed line was calculated by finding the value of ρ_p^{MF} which minimized the Jensen-Shannon divergence between the ρ_p^N and the inferred ρ_p posterior. The dashed red line in the *Left panel* show the inferred ρ_p distributions calculated using the samples from Colleoni *et al.* [42].

Analysis	ρ_{33}	$P_{33}(\%)$	ρ_p	$P_p(\%)$
LVK	$3.5^{+0.8}_{-1.2}$	0.24	$3.0^{+1.6}_{-1.5}$	1.3
Colleoni <i>et al.</i>	$3.5^{+1.1}_{-1.2}$	0.030	$2.5^{+1.8}_{-1.4}$	5.1
Nitz <i>et al.</i>	$3.4^{+1.3}_{-1.3}$	-	$2.3^{+1.8}_{-1.3}$	-
Zevin <i>et al.</i>	$3.5^{+0.9}_{-1.2}$	-	$2.9^{+1.7}_{-1.6}$	-

TABLE II. Table as in Table I but showing only the inferred posteriors and p-values for GW190412. We compare analyses from the LVK [28, 58], Colleoni *et al.* [42, 61], Nitz *et al.* [39] and Zevin *et al.* [62, 63]. We calculate ρ_{33} and ρ_p for Zevin *et al.* by using posterior samples obtained from the “Model A” analysis since the priors are the same as those used in Ref. [28]. We equally combined the posterior samples obtained with the SEOBNRv4PHM [64] and IMRPHENOMPv3HM [65] waveform models as was done in Ref. [28].

GW190814-like system with in-plane spin $0 < \chi_p < 0.1$ is indistinguishable from a non-precessing system based on the difference in Bayesian evidence.

2. GW190412

GW190412 was the first detection of a BBH with conclusively unequal component masses: $30.1^{+4.6}_{-5.3} M_\odot$ and $8.3^{+1.6}_{-0.9} M_\odot$ and the first observation where subdominant multipole moments were clearly observed. GW190412 was also the first observation where an informative precession measurement was inferred, with the posterior deviating significantly from the prior [28].

Several groups later re-analysed GW190412 and found similar results [39, 42, 43, 62].

We infer that GW190412 has the second most significant measurement of ρ_{33} in O3a, and that the inferred ρ_{33} measurement is inconsistent with noise with $P_{33} = 0.2\%$. This suggests that higher multipoles are present in the system, a result consistent with parameter estimation studies from Refs. [28, 42, 43]. In Table II, we present results for the significance of the (3, 3) multipole from several different analyses of GW19041, and consistently show that it is found with a significant SNR.⁷

We find that the evidence for precession in GW190412 is dependent on which Bayesian analysis is considered. We calculate that GW190412 shows marginal evidence for precession when using data from the initial analysis conducted by the LVK [28]. We find that the inferred precession SNR can be reproduced from noise in only 1 in every 100 cases, see Figure 3. However, when using data produced from a re-analysis of GW190412 using the latest suite of Phenomenological waveform models (PHENOMX [67–71]) [42, 61], hereafter Colleoni *et al.*, GW190412 shows low evidence for precession since the inferred ρ_p is smaller than that reported by the LVK and can be reproduced from noise in 1 in every 20 cases. The smaller ρ_p is a consequence of inferring a lower in-plane spin, as shown in Figure 4.

⁷ Islam *et al.* [43] also re-analysed GW190412 using the NR-SUR7DQ4 waveform model [66] but their samples are not publicly available and therefore not included in this work.

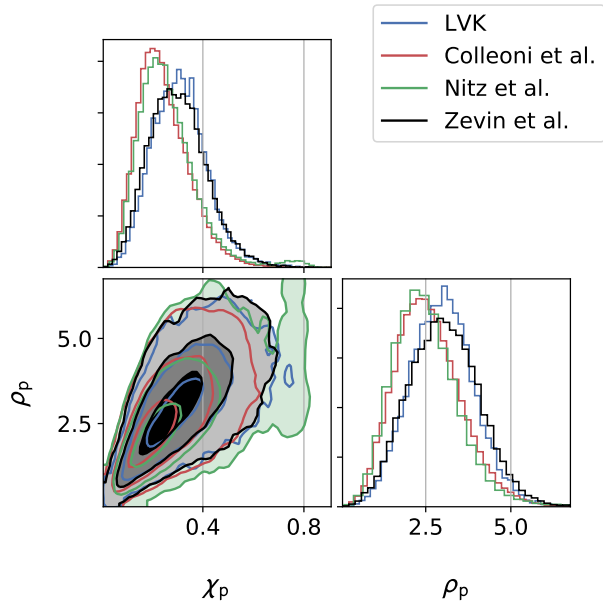


FIG. 4. Corner plot comparing the inferred χ_p and ρ_p for GW190412 from the LVK [28, 58], Colleoni *et al.* [42, 61], Nitz *et al.* [39] and Zevin *et al.* [62, 63]. Shading shows the 1 σ , 3 σ and 5 σ confidence intervals.

Nitz *et al.* [39] and Zevin *et al.* [62] also performed independent analyses of GW190412, and the results for ρ_p are included in Table II and Figure 4. However, since they did not release results for aligned-spin waveform models, we are unable to calculate p-values for the evidence of precession in the observed GW signal. Nonetheless, the inferred ρ_p and χ_p distributions from Nitz *et al.* and Zevin *et al.* are comparable to the measurements reported in Colleoni *et al.* and the LVK respectively.

Colleoni *et al.* and Nitz *et al.* both used the IMR-PHENOMXPHM waveform model [69] for the Bayesian inference while the LVK and Zevin *et al.* used a combination of the IMRPHENOMPV3HM [65] and SEOBNRV4PHM [64] waveform models. This suggests that the differences we see between interpretations could either be a consequence of waveform systematics, difficulties in sampling the complex parameter space or sampler differences.

3. GW190519_153544 and GW190929_012149

GW190519_153544 originated from a binary with relatively high total mass, 50% posterior probability for $M > 100M_\odot$, and with spins preferentially aligned

with the orbital angular momentum, $\chi_{\text{eff}} = 0.31^{+0.20}_{-0.22}$. GW190519_153544 shows marginal evidence for higher order multipoles since there is a 2% probability of recovering the inferred ρ_{33} from noise, see Figure 5. The inferred properties of the signal change significantly when higher harmonics are considered (as shown in Figure 13 of Ref. [50]). Specifically, the mass ratio is constrained more tightly and the binary is inferred to be edge-on, rather than face-on. Both of these effects are consistent with the presence of higher harmonics in the signal. However, as shown in Figure 2, when GW190412 and GW190814 are removed the population, the observed ρ_{33} is consistent with the population expectations from a no-signal hypothesis.

GW190929_012149 also shows marginal evidence for higher-order multipoles, with $\rho_{33} = 2.0^{+1.6}_{-1.5}$ which is expected from noise only in 4% of cases. Inclusion of higher harmonics in parameter recovery does lead to improved inference of the mass ratio, but has little impact on the measured orientation. Again, while a 4% chance might be significant for a single event, this observation is consistent with being an outlier in a population of thirty events.

Neither GW190519_153544 or GW190929_012149 show strong evidence for precession, as the inferred ρ_p is consistent with noise ($P_p \sim 13\%$ for both events).

4. GW190915_235702

In our analysis, GW190915_235702 has the second-largest evidence of precession in O3a with $P_p = 4\%$. GW190915_235702 originated from a BBH with component masses $35.3^{+9.5}_{-6.4} M_\odot$ and $24.4^{+5.6}_{-6.1} M_\odot$. The LVK analysis shows signs of precession in GW190915_235702, with $\chi_p \approx 0.6^{+0.3}_{-0.4}$ measured to be larger than prior expectations, see Figure 11 of Ref. [38]. In addition, when incorporating precession, the binary’s inclination is constrained to be away from face-on.

GW190915_235702 has no evidence for subdominant multipole moments with $P_{33} = 50\%$. The lack of evidence for subdominant multipole moments is consistent with the findings from the LVK analysis which found that the effect of higher modes is either negligible or subdominant to the systematics between precessing non-higher order multipole waveforms [38].

c. An investigation of GW190521

GW190521 is the most massive binary contained in GWTC-2.1. An initial analysis conducted by the LVK

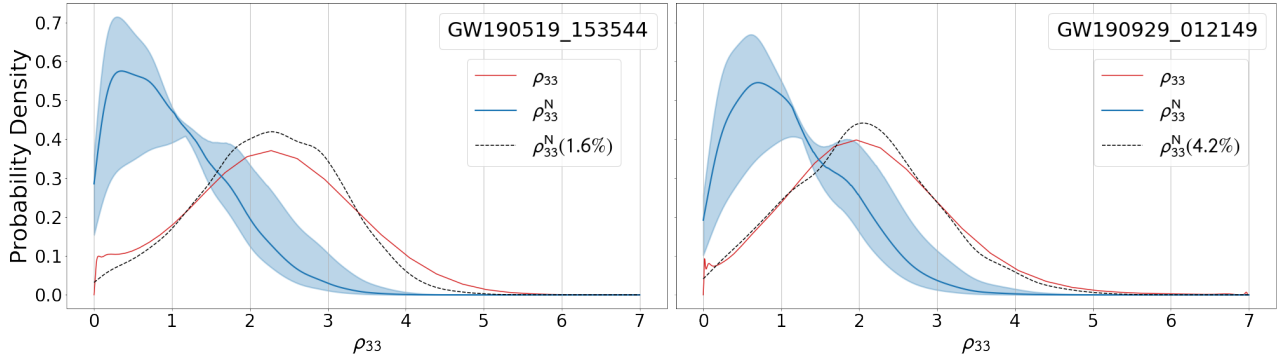


FIG. 5. ρ_{33} for *Left*: GW190519_153544 and *Right*: GW190929_012149. The blue line shows the expected distribution of ρ_{33} in a stretch of noisy data, ρ_{33}^N . The blue shaded region shows the 1σ uncertainty of ρ_{33}^N , the grey dotted line shows the expected ρ_{33}^N distribution in 10% of cases and the black dashed line shows the expected ρ_{33}^N distribution in *Left*: 1.5% and *Right*: 10% of cases. The black dashed line was calculated by finding the ρ_1^{MF} which minimized the Jensen-Shannon divergence between the ρ_{33}^N and the inferred ρ_{33} posterior.

argued that GW190521 provided the first evidence of a new population of black holes that resist straightforward interpretation as supernova remnants, with at least one black hole lying firmly in the pulsational pair-instability mass gap ($\sim 65 - 120 M_\odot$) [55, 72]. It was found that GW190521 was consistent with component masses $85^{+21}_{-14} M_\odot$ and $66^{+17}_{-18} M_\odot$. Nitz *et al.* [73] later challenged this view, showing that it is possible to obtain parameter estimates consistent with component masses that instead straddle this gap. Using a uniform in mass-ratio prior, GW190521’s mass posterior was multi-modal with additional modes at larger mass ratio, $q \sim 6$ and $q \sim 10$, and less support for equal mass ratio systems. Constraints on the mass ratio imposed by the initial analysis [38, 55, 72] ruled out any possibility of sampling this high mass ratio region of the parameter space. It was later discovered that the waveform approximant used by Nitz *et al.* did not accurately account for possibility of transitional precession [16, 39]. Nitz *et al.*’s alternative interpretation of GW190521 was therefore later revised in Ref. [39] with the high mass ratio $q \sim 10$ peak no longer significantly supported, while the mode at $q \sim 6$ remained. GW190521 may therefore have originated from either a near equal mass system, where the SNR in both the (3, 3) multipole [22] and precession [30] are expected to be small, or an unequal mass ratio system, where it is likely that higher order multipole and precession effects could be directly measured.

As might be expected, we obtain different results for the power in the (3, 3) multipole from the LVK and Nitz *et al.* samples. We infer that GW190521 has a measurable (3, 3) multipole if we use the posterior samples obtained from Nitz *et al.* ($\rho_{33} = 2.4^{+2.2}_{-2.0}$)

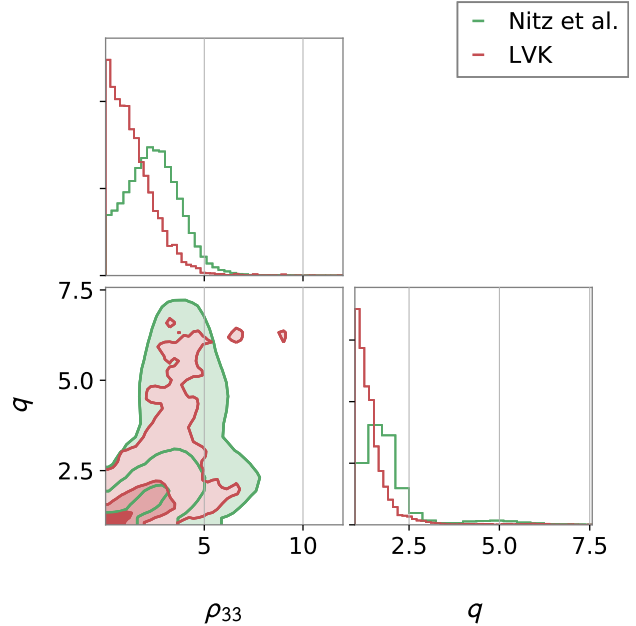


FIG. 6. Corner plot showing the inferred mass ratio and ρ_{33} for the reanalysis of GW190521 by Nitz *et al.* [39] compared to the results from the LVK [38, 55, 58, 72]. Shading shows the 1σ , 3σ and 5σ confidence intervals.

otherwise the inferred ρ_{33} is consistent with Gaussian noise ($\rho_{33} = 1.2^{+2.4}_{-1.1}$). Figure 6 shows that the inferred ρ_{33} in the analyses is correlated with the mass ratio, where more unequal masses are consistent with a larger ρ_{33} . Nitz *et al.* infer a non-equal mass ratio system, $q = 1.8^{+2.8}_{-0.6}$ [39], while the analysis from the LVK infers

$q = 1.3_{-0.3}^{+1.2}$ [38, 55, 72]. It is the extra likelihood from the measurement of the (3,3) multipole that is key to the Nitz *et al.* reinterpretation of GW190521 as an unequal mass binary.

GW190521 has the largest inferred in-plane spins of any event observed in GWTC-2.1 with $\chi_p = 0.68_{-0.44}^{+0.26}$ and $\chi_p = 0.5_{-0.33}^{+0.31}$ as reported by the LVK [38, 55, 72] and Nitz *et al.* respectively. However, GW190521 shows no evidence for precession in our analysis, with $\rho_p = 0.7_{-0.6}^{+1.4}$ and $\rho_p = 1.1_{-0.9}^{+2.8}$ respectively. While initially surprising, the lack of observable power in precession is a consequence of the high mass of the system. The observed waveform contains only about four cycles (two orbits) in the detectors' sensitive frequency band. As a result, GW190521 undergoes significantly less than one precession cycle in band and the two leading precession harmonics are highly degenerate. Thus, there is very little power orthogonal to the dominant harmonic, leading to a small inferred value of ρ_p .

In order to explore the differences between the LVK and Nitz *et al.* samples, we investigate whether the inferred ρ_{33} is consistent with the observed GW strain data [74, 75] by directly extracting the SNR in the (3, 3) multipole through matched filtering [76–78]. Since the relative power in the (2, 2) and (3, 3) multipoles depends strongly on both the mass-ratio and inclination of the system [see e.g. 22], we can then use the extracted SNR in the (3, 3) multipole to identify the region of parameter space consistent with the observed GW strain data and compare to the two distinct parameter estimation results. Matched filtering is a standard procedure when searching for GW from binary mergers [see e.g. 79–91], however in most cases only the SNR in the dominant (2, 2) multipole is typically calculated [see e.g. 9, 11, 38, 39, 92].

In Section II a, we argued that the impact of both precession and higher harmonics will be sub-leading and therefore we can filter for each independently. To do so, we first identify the point in the aligned-spin parameter space which gives the largest network SNR. Then, using these parameters, we calculate the waveform for the higher multipoles, (3,3), (4,4) and (2,1), as well as the leading order precession correction. Since the other harmonics are not orthogonal to the (2,2), we first project the waveform onto the space orthogonal to the (2,2) before filtering. This is particularly significant for (2,1) harmonic, which has a 0.7 overlap with the (2,2). The two leading precession harmonics are so close to degenerate (with $> 95\%$ overlap between them) that we cannot reliably evaluate the precession SNR. We then filter the orthogonal parts of each harmonic against the data from each detector and calculate the complex SNR in the harmonic at the

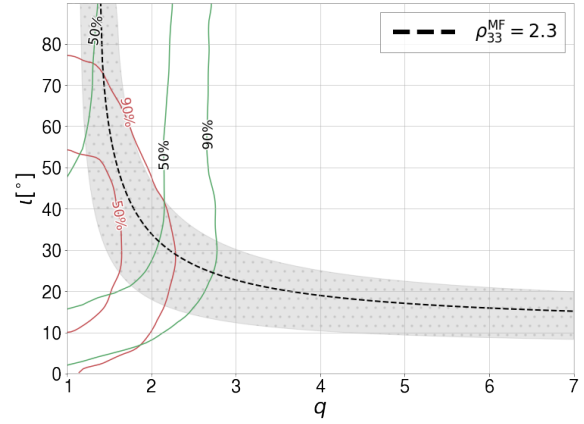


FIG. 7. Region of the inclination ι and mass ratio q parameter space consistent with a matched filter SNR in the (3, 3) multipole $\rho_{33}^{\text{MF}} = 2.3$ (dashed black line) and a 1σ uncertainty band (shaded grey region). Red and green contours show the 50% and 90% credible intervals consistent with the LVK analysis [38, 55, 58, 72] and the Nitz *et al.* analysis [39] of GW190521 respectively.

coalescence time. To calculate the network SNR in each harmonic we project to the space where the relative amplitudes in each detector are consistent with the leading (2,2) harmonic. Although this does not take into account each detector's response function and their different PSDs, our simplification only introduces at most a 5% error in the inferred higher multipole SNR.

We obtain a matched filter SNR of $\rho_{33} = 2.3$ using the above procedure. The relative SNR in the (2,2) and (3,3) harmonics depends upon the orientation of the signal — the SNR of the (3,3) scales with $\sin \iota$ relative to the (2,2) — as well as the mass ratio — with the relative SNR of the (3,3) larger for more unequal masses. Consequently, we can identify a region of parameter space consistent with these SNRs. The result is shown in Figure 7. The band is broadly consistent with the Nitz *et al.* results at small mass ratios, while the LVK results prefer lower mass ratios — as might be expected due to the smaller inferred value of ρ_{33} . We note that our analysis is *only* using the relative SNRs in the two modes, so cannot be expected to fully reproduce the system parameters. Higher mass ratios will be excluded by the fact that the (2,2) waveform is not a good match with the data.

We find limited power in the (4,4) harmonic, with $\rho_{44} = 1.2$, which is consistent with noise fluctuations. However, there is significant power in the (2,1) har-

monic, with $\rho_{21} = 3.4$. This is *inconsistent* with the known amplitude of the (2,1) harmonic across the parameter space: there is no combination of mass ratio and inclination that would give sufficient power in the (2,1) harmonic to yield this SNR. The observed ρ_{21} is also unlikely to be a noise fluctuation since we are unable to reproduce $\rho_{21} > 3.4$ when performing the above procedure on the best matching template injected into 100 different realizations of Gaussian noise. This therefore suggests that the significant ρ_{21} may be a sign of physics which isn't included in the waveform model. Several alternatives to precession have been suggested for this system, including possible evidence for eccentricity [93, 94] and head-on collisions [95].

The second, high mass ratio peak observed in Nitz *et al.* is inconsistent with the extracted matched filter SNR in the (3, 3) multipole. The secondary peak correspond to binaries with $q \sim 6$, large, partially misaligned spins viewed close to edge-on. For such a system, all five of the precession harmonics are important and, therefore, our aligned spin analysis with higher harmonic and precession corrections is not valid in that region of the parameter space.

Understanding if GW190521 has a measurable (3, 3) multipole is key for understanding the binary's formation mechanism. If GW190521 has a measurable (3,3) multipole, it is unlikely to originate from an equal mass system. The preferred formation mechanism has been investigated previously with some authors suggesting that GW190521 may be a result of a hierarchical merger [96] (although the initial LVK analysis found no conclusive evidence that GW190521 resulted from a hierarchical merger [55]). An unequal mass ratio provides evidence that one component is the result of a previous merger [96]. Possible evidence for eccentricity, or a head-on collision, would bolster a hierarchical interpretation [93, 94].

IV. Discussion

We calculated the inferred SNR in the subdominant multipole moments, ρ_{lm} (for $(\ell, |m|) \in \{(2, 1), (3, 3), (4, 4)\}$), and from precession, ρ_p , for all BBH candidates in GWTC-2.1 that were observed during O3a. We determined which events show evidence for subdominant multipole moments and precession by comparing the inferred SNRs with predicted distributions expected from noise alone. We found that most BBHs in O3a show minimal evidence for subdominant multipole moments, but there are two notable exceptions. GW190412 and GW190814 show significant evidence for a (3,3) multipole, while GW190519_153544

and GW190929_012149 show marginal evidence for the (3, 3) multipole. We also found that no BBH observed in O3a shows significant evidence for higher order multipole content beyond $\ell = 3$. We found that most BBHs in O3a show no evidence for precession. However, we found that GW190412 may have originated from a precessing binary system, with the observed result unlikely to be due to noise alone. However, when viewed as part of the population of events from GWTC-2.1, the observation is consistent with expectations from noise fluctuations. GW190915_235702 shows marginal evidence for precession, which is again not significant when viewed from a population perspective.

The interpretation of GW190521 is more complex, and is dependent upon the parameter estimation results which are used. The LVK analysis shows no evidence for higher harmonics or precession, while the Nitz *et al.* analysis shows power in the (3,3) harmonic. For this event, we were also able to directly calculate the matched filter SNRs directly from the data and show that we do obtain power in the (3,3) harmonic, which lends strength to the argument that the binary had unequal masses. However, we also find significant SNR in the (2,1) harmonic, which is inconsistent with physical expectations. One explanation for this might be that GW190521 originated from an eccentric merger [93, 94] in which case the waveform model we used would not contain the relevant physics.

The method we have presented is straightforward, and clearly identifies the evidence for subdominant multipole moments and precession from the observed GW signals. As demonstrated in our analysis of GW190521, it is possible to calculate the SNR in higher-multipoles and precession directly from the data — rather than using the results of parameter estimation analyses as we have done for the rest of the events in the paper. This opens up the possibility of using the observed SNR in higher multipoles and precession to infer the properties of the observed binary, in advance of a detailed parameter estimation analysis. A similar approach has been suggested proposed in Ref. [17], where the authors demonstrated that re-weighting posteriors inferred with a (2,2) only waveform model based on the full likelihood gave results that closely match those obtained from an analysis with waveform models including higher order multipoles. In principle, this should enable the estimation of parameters, including the effects of precession and higher multipoles, using posteriors computed with a simpler waveform model supplemented by the measured SNRs in higher multipoles and precession. In the future we wish to expand this method and calculate the SNR in the second, sub-

dominant GW polarization as the clear observation of two polarizations is also important for breaking degeneracies between parameters [97].

V. Acknowledgements

We are grateful to Duncan Brown, Davide Gerosa, Bernard Schutz and Vivien Raymond for discussions during C. Hoy’s and C. Mills’s Ph.D. defences where this work was first presented. We also thank Mark Hannam, Alex Nitz and Jonathan Thompson for useful discussions and N V Krishnendu for comments on this manuscript. This work was supported by Science and Technology Facilities Council (STFC) grant ST/N005430/1 and European Research Council (ERC) Consolidator Grant 647839 and we are grateful for computational resources provided by Cardiff University and LIGO Laboratory and supported by STFC grant ST/N000064/1 and National Science Foundation Grants PHY-0757058 and PHY-0823459.

This research has made use of data, software and/or web tools obtained from the Gravitational Wave Open Science Center (<https://www.gw-openscience.org>), a service of LIGO Laboratory, the LIGO Scientific Collaboration and the Virgo Collaboration. LIGO is funded by the U.S. National Science Foundation. Virgo is funded by the French Centre National de Recherche Scientifique (CNRS), the Italian Istituto Nazionale della Fisica Nucleare (INFN) and the Dutch Nikhef, with contributions by Polish and Hungarian institutes.

Plots were prepared with Matplotlib [98], Corner (<https://corner.readthedocs.io>) [99] and PESUMMARY [59]. Functions within PYCBC [87] were used to perform the matched filtering described in Section IIIc and LALSUITE [100], NUMPY [101] and SCIPY [102] were used during the analysis.

A. Posterior samples used

For all calculations we used posterior samples reweighed to a flat-in-comoving-volume prior to remain consistent with the results in Refs [38, 40]. For the majority of events we used the same posterior samples as those published in GWTC-2 and GWTC-2.1 (the “PublicationSamples” and “PrecessingSpin-

IMRHM.comoving” datasets respectively). In cases where these datasets did not correspond to samples obtained with a precessing higher-order multipole approximant we used the “C01:SEOBNRv4PHM” dataset which includes posterior samples obtained with the SEOBNRv4PHM [64] (precessing and higher-order multipole) approximant for both analyses⁸.

Since we calculate the inferred $\rho_{\ell m}$ and ρ_p with samples obtained from a precessing higher order multipole waveform model, we calculate the *informed* prior using samples obtained with a precessing non-higher order multipole and aligned-spin higher order multipole waveform model in order to ensure that the noise distribution is not biased by the absence of precession and higher order multipoles respectively. Although both Ref. [38] and Ref. [40] performed parameter estimation using multiple models, Ref. [40] only analysed each candidate with precessing higher order multipole waveform models while Ref. [38] analysed each candidate with aligned-spin and precessing waveform models, see Table VIII of [38].

Due to the lack of samples, we are unable to calculate an *informed* prior, and hence noise distribution, for candidates specific to Ref. [40]. For candidates described in Ref. [38] we were able to use samples obtained with a precessing non-higher order multipole waveform model (the “PrecessingSpinIMR” dataset) to calculate the *informed* prior for $\rho_{\ell m}$ but, because not every candidate was analysed with an aligned-spin higher order multipole waveform model, we generally used samples obtained with an aligned-spin non-higher order multipole waveform model to calculate the *informed* prior for ρ_p (the “AlignedSpinIMR” dataset). We expect that using an aligned-spin non-higher order multipole waveform model will not cause a significance difference in the obtained noise distribution for the absence of precession, since for the majority of cases the power from higher order multipoles is expected to be small and therefore parameter estimates comparable. For GW190412 and GW190814, both of which exhibit strong evidence for subdominant multipole moments [28, 29], we were able to use samples obtained with an aligned-spin higher order multipole waveform model (the “AlignedSpinIMRHM” dataset) to calculate the expected noise distribution for the absence of precession.

⁸ This included: GW190707.093326, GW190720.000836, GW190728.064510, GW190915.235702, GW190924.021846,

GW190929.012149, GW190930.133541, see Table VIII of Ref. [38]

-
- [1] J. Aasi et al. Advanced LIGO. *Class. Quant. Grav.*, 32:074001, 2015.
- [2] F Acernese, M Agathos, K Agatsuma, D Aisa, N Allemandou, A Allocca, J Amarni, P Astone, G Balestri, G Ballardini, et al. Advanced virgo: a second-generation interferometric gravitational wave detector. *Classical and Quantum Gravity*, 32(2):024001, 2014.
- [3] B. P. Abbott et al. Observation of Gravitational Waves from a Binary Black Hole Merger. *Phys. Rev. Lett.*, 116(6):061102, 2016.
- [4] B. P. Abbott et al. Binary Black Hole Mergers in the first Advanced LIGO Observing Run. *Phys. Rev.*, X6(4):041015, 2016. [erratum: *Phys. Rev.* X8,no.3,039903(2018)].
- [5] B. P. Abbott et al. GW151226: Observation of Gravitational Waves from a 22-Solar-Mass Binary Black Hole Coalescence. *Phys. Rev. Lett.*, 116(24):241103, 2016.
- [6] Benjamin P. Abbott et al. GW170104: Observation of a 50-Solar-Mass Binary Black Hole Coalescence at Redshift 0.2. *Phys. Rev. Lett.*, 118(22):221101, 2017. [Erratum: *Phys. Rev. Lett.* 121, 129901 (2018)].
- [7] B. P. Abbott et al. GW170608: Observation of a 19-solar-mass Binary Black Hole Coalescence. *Astrophys. J. Lett.*, 851:L35, 2017.
- [8] Benjamin P Abbott, Richard Abbott, TD Abbott, F Acernese, K Ackley, C Adams, T Adams, P Addesso, Rana X Adhikari, VB Adya, et al. Gw170814: a three-detector observation of gravitational waves from a binary black hole coalescence. *Physical review letters*, 119(14):141101, 2017.
- [9] BP Abbott, R Abbott, TD Abbott, S Abraham, F Acernese, K Ackley, C Adams, RX Adhikari, VB Adya, C Affeldt, et al. Gwtc-1: A gravitational-wave transient catalog of compact binary mergers observed by ligo and virgo during the first and second observing runs. *Physical Review X*, 9(3):031040, 2019.
- [10] B. P. Abbott et al. GW170817: Observation of Gravitational Waves from a Binary Neutron Star Inspiral. *Phys. Rev. Lett.*, 119(16):161101, 2017.
- [11] Alexander H Nitz, Thomas Dent, Gareth S Davies, Sumit Kumar, Collin D Capano, Ian Harry, Simone Mozzon, Laura Nuttall, Andrew Lundgren, and Márton Tápai. 2-ogc: Open gravitational-wave catalog of binary mergers from analysis of public advanced ligo and virgo data. *The Astrophysical Journal*, 891(2):123, 2020.
- [12] Tejaswi Venumadhav, Barak Zackay, Javier Roulet, Liang Dai, and Matias Zaldarriaga. New binary black hole mergers in the second observing run of advanced ligo and advanced virgo. *Physical Review D*, 101(8):083030, 2020.
- [13] Barak Zackay, Tejaswi Venumadhav, Liang Dai, Javier Roulet, and Matias Zaldarriaga. Highly spinning and aligned binary black hole merger in the advanced ligo first observing run. *Physical Review D*, 100(2):023007, 2019.
- [14] Barak Zackay, Liang Dai, Tejaswi Venumadhav, Javier Roulet, and Matias Zaldarriaga. Detecting gravitational waves with disparate detector responses: two new binary black hole mergers. *arXiv preprint arXiv:1910.09528*, 2019.
- [15] K. S. Thorne. Multipole Expansions of Gravitational Radiation. *Rev. Mod. Phys.*, 52:299–339, 1980.
- [16] Theocharis A. Apostolatos, Curt Cutler, Gerald J. Sussman, and Kip S. Thorne. Spin induced orbital precession and its modulation of the gravitational wave forms from merging binaries. *Phys. Rev.*, D49:6274–6297, 1994.
- [17] Ethan Payne, Colm Talbot, and Eric Thrane. Higher order gravitational-wave modes with likelihood reweighting. *Phys. Rev. D*, 100(12):123017, 2019.
- [18] Stephen Fairhurst, Rhys Green, Mark Hannam, and Charlie Hoy. When will we observe binary black holes precessing? *arXiv preprint arXiv:1908.00555*, 2019.
- [19] Katerina Chatziioannou et al. On the properties of the massive binary black hole merger GW170729. *Phys. Rev. D*, 100(10):104015, 2019.
- [20] Maite Mateu-Lucena, Sascha Husa, Marta Colleoni, Héctor Estellés, Cecilio García-Quirós, David Keitel, Maria de Lluc Planas, and Antoni Ramos-Buades. Adding harmonics to the interpretation of the black hole mergers of GWTC-1. 5 2021.
- [21] Horng Sheng Chia, Seth Olsen, Javier Roulet, Liang Dai, Tejaswi Venumadhav, Barak Zackay, and Matias Zaldarriaga. Boxing Day Surprise: Higher Multipoles and Orbital Precession in GW151226. 5 2021.
- [22] Cameron Mills and Stephen Fairhurst. Measuring gravitational-wave higher-order multipoles. *Phys. Rev. D*, 103(2):024042, 2021.
- [23] J. Veitch et al. Parameter estimation for compact binaries with ground-based gravitational-wave observations using the LALInference software library. *Phys. Rev. D*, 91(4):042003, 2015.
- [24] Jacob Lange, Richard O’Shaughnessy, and Monica Rizzo. Rapid and accurate parameter inference for coalescing, precessing compact binaries. 5 2018.
- [25] Gregory Ashton et al. BILBY: A user-friendly Bayesian inference library for gravitational-wave astronomy. *Astrophys. J. Suppl.*, 241(2):27, 2019.
- [26] Lionel London, Sebastian Khan, Edward Fauchon-Jones, Cecilio García, Mark Hannam, Sascha Husa, Xisco Jiménez-Forteza, Chinmay Kalaghatgi, Frank Ohme, and Francesco Pannarale. First higher-multipole model of gravitational waves from spinning and coalescing black-hole binaries. *Phys. Rev. Lett.*, 120(16):161102, 2018.
- [27] Chinmay Kalaghatgi, Mark Hannam, and Vivien

- Raymond. Parameter estimation with a spinning multimode waveform model. *Phys. Rev. D*, 101(10):103004, 2020.
- [28] R. Abbott et al. GW190412: Observation of a Binary-Black-Hole Coalescence with Asymmetric Masses. *Phys. Rev. D*, 102(4):043015, 2020.
- [29] R. Abbott et al. GW190814: Gravitational Waves from the Coalescence of a 23 Solar Mass Black Hole with a 2.6 Solar Mass Compact Object. *Astrophys. J. Lett.*, 896(2):L44, 2020.
- [30] Rhys Green, Charlie Hoy, Stephen Fairhurst, Mark Hannam, Francesco Pannarale, and Cory Thomas. Identifying when Precession can be Measured in Gravitational Waveforms. *Phys. Rev. D*, 103(12):124023, 2021.
- [31] Larne Pekowsky, James Healy, Deirdre Shoemaker, and Pablo Laguna. Impact of higher-order modes on the detection of binary black hole coalescences. *Phys. Rev. D*, 87(8):084008, 2013.
- [32] Vijay Varma, Parameswaran Ajith, Sascha Husa, Juan Calderon Bustillo, Mark Hannam, and Michael Pürrer. Gravitational-wave observations of binary black holes: Effect of nonquadrupole modes. *Phys. Rev. D*, 90(12):124004, 2014.
- [33] Juan Calderón Bustillo, Sascha Husa, Alicia M. Sintes, and Michael Pürrer. Impact of gravitational radiation higher order modes on single aligned-spin gravitational wave searches for binary black holes. *Phys. Rev. D*, 93(8):084019, 2016.
- [34] Collin Capano, Yi Pan, and Alessandra Buonanno. Impact of higher harmonics in searching for gravitational waves from nonspinning binary black holes. *Phys. Rev. D*, 89(10):102003, 2014.
- [35] Alberto Vecchio. Lisa observations of rapidly spinning massive black hole binary systems. *Physical Review D*, 70(4):042001, 2004.
- [36] Ryan N. Lang and Scott A. Hughes. Measuring coalescing massive binary black holes with gravitational waves: The Impact of spin-induced precession. *Phys. Rev.*, D74:122001, 2006. [Erratum: *Phys. Rev.* D77,109901(2008)].
- [37] Geraint Pratten, Patricia Schmidt, Riccardo Buscicchio, and Lucy M. Thomas. Measuring precession in asymmetric compact binaries. *Phys. Rev. Res.*, 2(4):043096, 2020.
- [38] R. Abbott, TD Abbott, S Abraham, F Acernese, K Ackley, A Adams, C Adams, RX Adhikari, VB Adya, C Affeldt, et al. Gwtc-2: Compact binary coalescences observed by ligo and virgo during the first half of the third observing run. *arXiv preprint arXiv:2010.14527*, 2020.
- [39] Alexander H. Nitz, Collin D. Capano, Sumit Kumar, Yi-Fan Wang, Shilpa Kastha, Marlin Schäfer, Rahul Dhurkunde, and Miriam Cabero. 3-OGC: Catalog of gravitational waves from compact-binary mergers. 5 2021.
- [40] R. Abbott et al. GWTC-2.1: Deep Extended Catalog of Compact Binary Coalescences Observed by LIGO and Virgo During the First Half of the Third Observing Run. 8 2021.
- [41] R. Abbott et al. GWTC-3: Compact Binary Coalescences Observed by LIGO and Virgo During the Second Part of the Third Observing Run. 11 2021.
- [42] Marta Colleoni, Maite Mateu-Lucena, Héctor Estellés, Cecilio García-Quirós, David Keitel, Geraint Pratten, Antoni Ramos-Buades, and Sascha Husa. Towards the routine use of subdominant harmonics in gravitational-wave inference: Reanalysis of GW190412 with generation X waveform models. *Phys. Rev. D*, 103(2):024029, 2021.
- [43] Tousif Islam, Scott E. Field, Carl-Johan Haster, and Rory Smith. Improved analysis of GW190412 with a precessing numerical relativity surrogate waveform model. *Phys. Rev. D*, 103(10):104027, 2021.
- [44] Collin D. Capano and Alexander H. Nitz. Binary black hole spectroscopy: a no-hair test of GW190814 and GW190412. *Phys. Rev. D*, 102(12):124070, 2020.
- [45] Mark Hannam, Charlie Hoy, Jonathan E. Thompson, Stephen Fairhurst, Vivien Raymond, and members of the LIGO. Measurement of general-relativistic precession in a black-hole binary. 12 2021.
- [46] R. Abbott et al. Population Properties of Compact Objects from the Second LIGO-Virgo Gravitational-Wave Transient Catalog. *Astrophys. J. Lett.*, 913(1):L7, 2021.
- [47] R. Abbott et al. The population of merging compact binaries inferred using gravitational waves through GWTC-3. 11 2021.
- [48] Stephen Fairhurst, Rhys Green, Charlie Hoy, Mark Hannam, and Alistair Muir. Two-harmonic approximation for gravitational waveforms from precessing binaries. *Phys. Rev. D*, 102:024055, 2020.
- [49] Joshua N Goldberg, Alan J MacFarlane, Ezra T Newman, Fritz Rohrlich, and EC George Sudarshan. Spins spherical harmonics and edth. *Journal of Mathematical Physics*, 8(11):2155–2161, 1967.
- [50] R. Abbott et al. GWTC-2: Compact Binary Coalescences Observed by LIGO and Virgo During the First Half of the Third Observing Run. *Phys. Rev. X*, 11:021053, 2021.
- [51] Soumen Roy, Anand S. Sengupta, and K. G. Arun. Unveiling the spectrum of inspiralling binary black holes. *Phys. Rev. D*, 103(6):064012, 2021.
- [52] S. Klimenko et al. Method for detection and reconstruction of gravitational wave transients with networks of advanced detectors. *Phys. Rev. D*, 93(4):042004, 2016.
- [53] R. Abbott et al. Observation of Gravitational Waves from Two Neutron Star–Black Hole Coalescences. *Astrophys. J. Lett.*, 915(1):L5, 2021.
- [54] Lawrence E. Kidder. Coalescing binary systems of compact objects to postNewtonian 5/2 order. 5. Spin effects. *Phys. Rev.*, D52:821–847, 1995.
- [55] R. Abbott et al. Properties and Astrophysical Implications of the 150 M_{\odot} Binary Black Hole Merger GW190521. *Astrophys. J. Lett.*, 900(1):L13, 2020.

- [56] Patricia Schmidt, Frank Ohme, and Mark Hannam. Towards models of gravitational waveforms from generic binaries II: Modelling precession effects with a single effective precession parameter. *Phys. Rev.*, D91(2):024043, 2015.
- [57] LIGO Scientific Collaboration and Virgo Collaboration. GWTC-2.1: Deep Extended Catalog of Compact Binary Coalescences Observed by LIGO and Virgo During the First Half of the Third Observing Run - Parameter Estimation Data Release, July 2021.
- [58] LIGO Scientific Collaboration and Virgo Collaboration. Gwtc-2 data release: Parameter estimation samples and skymaps, March 2021.
- [59] Charlie Hoy and Vivien Raymond. PESummary: the code agnostic Parameter Estimation Summary page builder. *SoftwareX*, 15:100765, 2021.
- [60] J. Lin. Divergence measures based on the shannon entropy. *IEEE Transactions on Information Theory*, 37(1):145–151, Jan 1991.
- [61] Marta Colleoni, Maite Mateu-Lucena, Héctor Estellés, Cecilio García-Quirós, David Keitel, Geraint Pratten, Antoni Ramos-Buades, and Sascha Husa. Data release for paper "Towards the routine use of subdominant harmonics in gravitational-wave inference: re-analysis of GW190412 with generation X waveform models", October 2020.
- [62] Michael Zevin, Christopher P. L. Berry, Scott Coughlin, Katerina Chatziioannou, and Salvatore Vitale. You Can't Always Get What You Want: The Impact of Prior Assumptions on Interpreting GW190412. *Astrophys. J. Lett.*, 899(1):L17, 2020.
- [63] Zevin, Coughlin, Berry, Chatziioannou, and Vitale. Gw190412 prior assumptions, June 2020.
- [64] Serguei Ossokine et al. Multipolar Effective-One-Body Waveforms for Precessing Binary Black Holes: Construction and Validation. *Phys. Rev. D*, 102(4):044055, 2020.
- [65] Sebastian Khan, Frank Ohme, Katerina Chatziioannou, and Mark Hannam. Including higher order multipoles in gravitational-wave models for precessing binary black holes. *Phys. Rev. D*, 101(2):024056, 2020.
- [66] Vijay Varma, Scott E. Field, Mark A. Scheel, Jonathan Blackman, Davide Gerosa, Leo C. Stein, Lawrence E. Kidder, and Harald P. Pfeiffer. Surrogate models for precessing binary black hole simulations with unequal masses. *Phys. Rev. Research.*, 1:033015, 2019.
- [67] Geraint Pratten, Sascha Husa, Cecilio Garcia-Quiros, Marta Colleoni, Antoni Ramos-Buades, Hector Estelles, and Rafel Jaume. Setting the cornerstone for a family of models for gravitational waves from compact binaries: The dominant harmonic for nonprecessing quasicircular black holes. *Phys. Rev. D*, 102(6):064001, 2020.
- [68] Cecilio García-Quirós, Marta Colleoni, Sascha Husa, Héctor Estellés, Geraint Pratten, Antoni Ramos-Buades, Maite Mateu-Lucena, and Rafel Jaume. Multimode frequency-domain model for the gravitational wave signal from nonprecessing black-hole binaries. *Phys. Rev. D*, 102(6):064002, 2020.
- [69] Geraint Pratten et al. Computationally efficient models for the dominant and subdominant harmonic modes of precessing binary black holes. *Phys. Rev. D*, 103(10):104056, 2021.
- [70] Héctor Estellés, Antoni Ramos-Buades, Sascha Husa, Cecilio García-Quirós, Marta Colleoni, Leila Haegel, and Rafel Jaume. Phenomenological time domain model for dominant quadrupole gravitational wave signal of coalescing binary black holes. *Phys. Rev. D*, 103(12):124060, 2021.
- [71] Héctor Estellés, Marta Colleoni, Cecilio García-Quirós, Sascha Husa, David Keitel, Maite Mateu-Lucena, Maria de Lluc Planas, and Antoni Ramos-Buades. New twists in compact binary waveform modelling: a fast time domain model for precession. 5 2021.
- [72] R. Abbott et al. GW190521: A Binary Black Hole Merger with a Total Mass of $150M_{\odot}$. *Phys. Rev. Lett.*, 125(10):101102, 2020.
- [73] Alexander H. Nitz and Collin D. Capano. GW190521 may be an intermediate mass ratio inspiral. *Astrophys. J. Lett.*, 907(1):L9, 2021.
- [74] Michele Vallisneri, Jonah Kanner, Roy Williams, Alan Weinstein, and Branson Stephens. The LIGO Open Science Center. *J. Phys. Conf. Ser.*, 610(1):012021, 2015.
- [75] Rich Abbott et al. Open data from the first and second observing runs of Advanced LIGO and Advanced Virgo. *SoftwareX*, 13:100658, 2021.
- [76] Bruce Allen, Warren G. Anderson, Patrick R. Brady, Duncan A. Brown, and Jolien D. E. Creighton. FIND-CHIRP: An Algorithm for detection of gravitational waves from inspiraling compact binaries. *Phys. Rev. D*, 85:122006, 2012.
- [77] Duncan A. Brown. Searching for gravitational radiation from binary black hole MACHOs in the galactic halo. Other thesis, 12 2004.
- [78] S. Babak et al. Searching for gravitational waves from binary coalescence. *Phys. Rev. D*, 87(2):024033, 2013.
- [79] K. Cannon, R. Cariou, A. Chapman, et al. Toward Early-Warning Detection of Gravitational Waves from Compact Binary Coalescence. *Astrophys. J.*, 748:136, 2012.
- [80] S. Privitera, S. R. P. Mohapatra, P. Ajith, et al. Improving the sensitivity of a search for coalescing binary black holes with nonprecessing spins in gravitational wave data. *Phys. Rev. D*, 89(2):024003, 2014.
- [81] C. Messick, K. Blackburn, P. Brady, et al. Analysis Framework for the Prompt Discovery of Compact Binary Mergers in Gravitational-wave Data. *Phys. Rev. D*, 95(4):042001, 2017.
- [82] Chad Hanna, Sarah Caudill, Cody Messick, Amit Reza, Surabhi Sachdev, Leo Tsukada, Kipp Cannon, Kent Blackburn, Jolien D. E. Creighton, Heather Fong, and et al. Fast evaluation of multidetector consistency for real-time gravitational wave searches.

- Phys. Rev. D*, 101(2):022003, January 2020.
- [83] S. Sachdev, S. Caudill, H. Fong, R. K. L. Lo, C. Messick, et al. The GstLAL Search Analysis Methods for Compact Binary Mergers in Advanced LIGO’s Second and Advanced Virgo’s First Observing Runs. *arXiv:1901.08580*, 2019.
- [84] S. A. Usman, A. H. Nitz, I. W. Harry, C. M. Biwer, D. A. Brown, et al. The PyCBC search for gravitational waves from compact binary coalescence. *CQGra*, 33(21):215004, 2016.
- [85] Alexander H. Nitz, Thomas Dent, Tito Dal Canton, Stephen Fairhurst, and Duncan A. Brown. Detecting binary compact-object mergers with gravitational waves: Understanding and Improving the sensitivity of the PyCBC search. *Astrophys. J.*, 849(2):118, 2017.
- [86] Alexander H. Nitz, Tito Dal Canton, Derek Davis, and Steven Reyes. Rapid detection of gravitational waves from compact binary mergers with PyCBC Live. *Phys. Rev. D*, 98(2):024050, 2018.
- [87] Alex Nitz, Ian Harry, Duncan Brown, Christopher M. Biwer, Josh Willis, Tito Dal Canton, Collin Capano, Larne Pekowsky, Thomas Dent, Andrew R. Williamson, et al. gwastro/pycbc: Pycbc release v1.15.2, December 2019.
- [88] T. Adams, D. Buskulic, V. Germain, G. M. Guidi, F. Marion, M. Montani, B. Mours, F. Piergiovanni, and G. Wang. Low-latency analysis pipeline for compact binary coalescences in the advanced gravitational wave detector era. *CQGra*, 33(17):175012, Sep 2016.
- [89] Shaun Hooper, Shin Kee Chung, Jing Luan, David Blair, Yanbei Chen, and Linqing Wen. Summed parallel infinite impulse response filters for low-latency detection of chirping gravitational waves. *Phys. Rev. D*, 86(2):024012, Jul 2012.
- [90] Y. Liu, Z. Du, S. K. Chung, S. Hooper, D. Blair, and L. Wen. GPU-accelerated low-latency real-time searches for gravitational waves from compact binary coalescence. *CQGra*, 29(23):235018, December 2012.
- [91] X. Guo, Q. Chu, S. K. Chung, Z. Du, L. Wen, and Y. Gu. GPU-acceleration on a low-latency binary-coalescence gravitational wave search pipeline. *CoPhC*, 231:62–71, October 2018.
- [92] Tejaswi Venumadhav, Barak Zackay, Javier Roulet, Liang Dai, and Matias Zaldarriaga. New search pipeline for compact binary mergers: Results for binary black holes in the first observing run of Advanced LIGO. *Phys. Rev. D*, 100(2):023011, 2019.
- [93] Isobel M. Romero-Shaw, Paul D. Lasky, Eric Thrane, and Juan Calderon Bustillo. GW190521: orbital eccentricity and signatures of dynamical formation in a binary black hole merger signal. *Astrophys. J. Lett.*, 903(1):L5, 2020.
- [94] V. Gayathri, J. Healy, J. Lange, B. O’Brien, M. Szczepańczyk, Imre Bartos, M. Campanelli, S. Klimentko, C. O. Lousto, and R. O’Shaughnessy. Eccentricity estimate for black hole mergers with numerical relativity simulations. *Nature Astronomy*, 6(3):344–349, 2022.
- [95] Juan Calderón Bustillo, Nicolas Sanchis-Gual, Alejandro Torres-Forné, and José A. Font. Confusing Head-On Collisions with Precessing Intermediate-Mass Binary Black Hole Mergers. *Phys. Rev. Lett.*, 126(20):201101, 2021.
- [96] Chase Kimball et al. Evidence for Hierarchical Black Hole Mergers in the Second LIGO–Virgo Gravitational Wave Catalog. *Astrophys. J. Lett.*, 915(2):L35, 2021.
- [97] Samantha A. Usman, Joseph C. Mills, and Stephen Fairhurst. Constraining the Inclinations of Binary Mergers from Gravitational-wave Observations. *Astrophys. J.*, 877(2):82, 2019.
- [98] J. D. Hunter. Matplotlib: A 2D Graphics Environment. *CSE*, 9:90–95, May 2007.
- [99] Daniel Foreman-Mackey. corner.py: Scatterplot matrices in python. *The Journal of Open Source Software*, 1(2):24, jun 2016.
- [100] LIGO Scientific Collaboration. LIGO Algorithm Library - LALSuite. free software (GPL), 2018.
- [101] Charles R. Harris, K. Jarrod Millman, Stéfan J. van der Walt, Ralf Gommers, Pauli Virtanen, David Cournapeau, Eric Wieser, Julian Taylor, Sebastian Berg, Nathaniel J. Smith, Robert Kern, Matti Picus, Stephan Hoyer, Marten H. van Kerkwijk, Matthew Brett, Allan Haldane, Jaime Fernández del Río, Mark Wiebe, Pearu Peterson, Pierre Gérard-Marchant, Kevin Sheppard, Tyler Reddy, Warren Weckesser, Hameer Abbasi, Christoph Gohlke, and Travis E. Oliphant. Array programming with NumPy. *Nature*, 585(7825):357–362, September 2020.
- [102] Pauli Virtanen, Ralf Gommers, Travis E. Oliphant, Matt Haberland, Tyler Reddy, David Cournapeau, Evgeni Burovski, Pearu Peterson, Warren Weckesser, Jonathan Bright, Stéfan J. van der Walt, Matthew Brett, Joshua Wilson, K. Jarrod Millman, Nikolay Mayorov, Andrew R. J. Nelson, Eric Jones, Robert Kern, Eric Larson, C J Carey, İlhan Polat, Yu Feng, Eric W. Moore, Jake VanderPlas, Denis Laxalde, Josef Perktold, Robert Cimrman, Ian Henriksen, E. A. Quintero, Charles R. Harris, Anne M. Archibald, Antônio H. Ribeiro, Fabian Pedregosa, Paul van Mulbregt, and SciPy 1.0 Contributors. SciPy 1.0: Fundamental Algorithms for Scientific Computing in Python. *Nature Methods*, 17:261–272, 2020.